Proceedings of the 29th Annual International
Conference of the IEEE EMBS
Cité Internationale, Lyon, France
August 23-26, 2007.

Precise 3-D localization of fluorescent probes without numerical fitting

Ting Sun and Sean B. Andersson

***Abstract*—We present an analytical algorithm for determining the position of a fluorescent probe in three dimensions (3-D) from a collection of measurements taken at different locations. This algorithm, fluoroBancroft, relies on the fact that the intensity point spread function depends only on the radial distance between the center of the focal point and the position of the fluorescent probe. We present a simulation study comparing the performance of the algorithm to the standard technique of fitting the data to a Gaussian profile. Our results indicate that in the 3-D case, the fluoroBancroft algorithm is able to localize the probe with an accuracy on the order of tens of nanometers using less than ten measurements (pixels). The Gaussian fitting procedure is unable to locate the probe even when using 36 measurements (the maximum number of measurements used in the simulations). Moreover the new technique is typically two orders of magnitude faster than the Gaussian fitting approach in terms of computation time. These results indicate the fluoroBancroft algorithm can be used effectively in a closed-loop controller to track the motion of single fluorescent probes in 3-D in a confocal microscope.**

I. Introduction

Single particle tracking in fluorescence microscopy has become an extremely important tool for understanding molecular processes [1], [2]. Particle tracking is typically achieved by analyzing a sequence of wide-field images obtained using a charge-coupled device (CCD) camera. Using techniques such as Gaussian fitting, the location of an isolated point-source can be determined in the plane with a precision on the order of a few nanometers. If limited to the focal plane, this technique can yield a temporal resolution on the order of milliseconds [3]. When extended to three dimensions, the temporal resolution is reduced to the range of seconds [4]. A confocal setup (and related techniques such as two-photon microscopy) operates in 3D and has a temporal resolution on the fluorescence measurements which is orders of magnitude faster than in wide-field imaging. In recent years, researchers have begun to develop algorithms for tracking single fluorescent probes in confocal and two-photon microscopes [5]–[7]. Because measurements are taken sequentially, it is important for high-speed tracking that the position of the probe can be determined rapidly and with only a few measurements.

One of the authors recently introduced the fluoroBancroft algorithm for estimating the location of a fluorescent probe in two dimensions (2-D) from intensity measurements. Its localization performance in the wide-field setting is comparable to the currently standard technique of fitting a Gaussian profile to the data [8] while in the confocal setting it has much better accuracy and requires measurements from only four to five locations in space [9]. Moreover, for the same amount of data, the computational speed is typically two orders of magnitude faster than the numerical fitting procedure. In this paper we extend the algorithm to 3-D localization in the confocal setting. The algorithm relies on the fact that the fluorescence intensity depends only on the distance to the probe. Therefore, a collection of measurements obtained at different locations can be interpreted as a set of range-only measurements. The fluoroBancroft algorithm is inspired by Bancroft's algorithm for solving a similar range-based localization problem in the global positioning system (GPS) [10].

Several algorithms exist for sub-diffraction limit localization and fundamental limits have been derived [11]. A common method is to fit the data to a Gaussian profile using a non-linear least-squares fit. This can provide precision on the order of 1-20 nm in a typical system [12], [13]. Most algorithms were developed for the wide-field setting where images are comprised of hundreds of pixels and has been used primarily in localizing a particle in the focal plane. In this paper we consider localization in 3-D based on confocal measurements and compare the performance of the fluoroBancroft algorithm to a Gaussian fitting approach. The simulation results indicate that fluoroBancroft can yield precise localization (with errors on the order of tens of nanometers) using less than ten measurements while the Gaussian fitting approach is unable to localize the fluorescent probe even when using 36 measurements (the maximum number used in this comparison).

II. The fluoroBancroft algorithm

In confocal fluorescence microscopy the output fluorescence intensity from a point source is the product of the illumination and detection intensity point spread functions (PSF) [14]. The intensity pattern is circularly symmetric and gives rise to the familiar Airy disk in the plane. Within the central disk, the intensity is well-approximated by a Gaussian. The PSF in the axial direction can also be approximated by a Gaussian within a limited range. Since in the tracking application it is reasonable to assume that the fluorescent tag will remain near the center of the focal point, we choose to model the intensity of a diffraction limited spot by

$$I_{psf} = me^{-\frac{(x-x_0)^2+(y-y_0)^2}{2\sigma^2}-\frac{(z-z_0)^2}{2\sigma_z}}. \tag{1}$$

Here, m is a scaling factor determined by the total number of photons emitted by the probe during the measurement period and 2σ is the full-width, half-maximum (FWHM) of the image spot in the focal plane, given by

$$2\sigma = \frac{1.22\lambda}{4\mathrm{N.A.}\ln 2} \tag{2}$$

T. Sun and S.B. Andersson are with the Department of Aerospace and Mechanical Engineering, Boston University, Boston, MA, 02215, USA. {tingsun,sanderss}@bu.edu

where N.A. is the numerical aperture of the objective. Similarly, $2\sigma_z$ is the full-width, half-maximum (FWHM) along the axial direction, taken here to be

$$2\sigma_z = \frac{1.4\lambda}{\text{N.A.}^2}. \tag{3}$$

The measured intensity is given by the true intensity together with background and shot noise. The background noise, arising primarily from unwanted excited and autofluorescence of the sample, is assumed to be constant across the field of view. For the purposes of position estimation, we model it as a Poisson random variable η_B with mean and variance equal to N_B. The statistics of the background noise can be determined experimentally and therefore we assume N_B is known. The shot noise is a Poisson process with a rate dependent on the total number of photons detected [1]. The model for the measured intensity with focal point located at (x_i, y_i, z_i) is

$$I_i = me^{-\frac{(x_i-x_0)^2+(y_i-y_0)^2}{2\sigma^2}-\frac{(z_i-z_0)^2}{2\sigma_z}} + \eta_B + \eta_{shot}. \tag{4}$$

Here i is indexing the measurement number. Scaling the axial coordinate by $z' = (\sigma/\sigma_z)\, z$, (4) can be rewritten as

$$I_i = me^{-\frac{r_i^2}{2\sigma^2}} + \eta_B + \eta_{shot} \tag{5}$$

where

$$r_i^2 = (x_i - x_0)^2 + (y_i - y_0)^2 + (z_i' - z_0')^2.$$

Taking the expected value of (4) and solving for r_i^2 yields

$$r_i^2 = 2\sigma^2 \ln(2m) - 2\sigma^2 \ln(I_i - 2N_B). \tag{6}$$

Note that because the background noise can be measured to determine N_B, the second term on the right-hand side of (6) is known. However m is related to the true intensity of the fluorescent probe and is therefore not known. Define

$$\begin{aligned} \Lambda &\triangleq \frac{1}{2}\left(x_0^2 + y_0^2 + z_0'^2\right),\ b \triangleq 2\sigma^2 \ln(2m) \\ P_i^2 &\triangleq 2\sigma^2 \ln(I_i - 2N_B), \\ \alpha_i &\triangleq \frac{1}{2}\left(x_i^2 + y_i^2 + z_i'^2 + P_i^2\right). \end{aligned}$$

Then (6) can be rewritten as

$$0 = \alpha_i + \Lambda - \begin{pmatrix} x_i & y_i & z_i' & 1 \end{pmatrix} \begin{pmatrix} x_0 \\ y_0 \\ z_0' \\ b \end{pmatrix}. \tag{7}$$

Stacking together n measurements yields

$$0 = \alpha + \Lambda e - B \begin{pmatrix} x_0 \\ y_0 \\ z_0 \\ b \end{pmatrix} \tag{8}$$

where

$$\alpha = \begin{pmatrix} \alpha_1 \\ \vdots \\ \alpha_n \end{pmatrix},\ e = \begin{pmatrix} 1 \\ \vdots \\ 1 \end{pmatrix},\ B = \begin{pmatrix} x_1 & y_1 & z_1' & 1 \\ & \vdots & & \\ x_n & y_n & z_n' & 1 \end{pmatrix}.$$

Pre-multiplying (8) by B^T and rearranging yields

$$\begin{pmatrix} x_0 & y_0 & z_0' & b \end{pmatrix}^T = B^\dagger (\alpha + \Lambda e) \tag{9}$$

where $B^\dagger = \left(B^T B\right)^{-1} B^T$ is the Moore-Penros pseudo-inverse of B. Notice that the unknown position (x_0, y_0) appears both on the left-hand side and on the right-hand side (through Λ). Since we are interested only in the location of the fluorescent probe, we isolate the position by pre-multiplying both sides of (9) by

$$Q = \begin{pmatrix} 1 & 0 & 0 & 0 \\ 0 & 1 & 0 & 0 \\ 0 & 0 & 1 & 0 \end{pmatrix}.$$

This yields

$$\begin{pmatrix} x_0 & y_0 & z_0' \end{pmatrix} = Q\left(B^\dagger (\alpha + \Lambda e)\right). \tag{10}$$

We now state an interesting property of $B^\dagger$.

Proposition 2.1: Let $e = (1, 1, \cdots, 1)^T$ and let A be an $n \times m$ matrix. Define $B = \begin{pmatrix} A & e \end{pmatrix}$. Then

$$B^\dagger e = \begin{pmatrix} 0 & 0 & \cdots & 0 & 1 \end{pmatrix}^T.$$

Proof: We have

$$B^T B = B^T \begin{pmatrix} A & e \end{pmatrix} = \begin{pmatrix} B^T A & B^T e \end{pmatrix}.$$

Thus $B^T e$ is the $(m+1)^{\text{th}}$ column of $B^T B$. Now

$$\begin{aligned} \mathbb{I} &= \left(B^T B\right)^{-1} \left(B^T B\right) \\ &= \begin{pmatrix} \left(B^T B\right)^{-1} B^T A & \left(B^T B\right)^{-1} B^T e \end{pmatrix}. \end{aligned}$$

Therefore $B^\dagger e = \left(B^T B\right)^{-1} B^T e$ is the last column of the identity matrix as claimed. ■

Applying this proposition to (10) results in

$$\begin{pmatrix} x_0 & y_0 & z_0' \end{pmatrix}^T = QB^\dagger \alpha. \tag{11}$$

To rescale the axial coordinate define

$$R = \begin{pmatrix} 1 & 0 & 0 \\ 0 & 1 & 0 \\ 0 & 0 & \frac{\sigma_z}{\sigma} \end{pmatrix}.$$

Then the solution to the localization problem is given by

$$\begin{pmatrix} x_0 & y_0 & z_0 \end{pmatrix}^T = RQB^\dagger \alpha. \tag{12}$$

Since B and α depend only on the measurements and the locations of those measurements, (12) determines the location of the fluorescent probe as a closed-form equation.

III. Simulation methods

To investigate the performance of the fluoroBancroft algorithm, we modeled a point source fluorescing at a wavelength of 540 nm at a rate of 40 photons/ms. The fluorescence was imaged using a 0.8 N.A., 20× magnification objective lens through a circular pinhole onto a point detector. The signal-to-noise ratio (SNR) depends on the pinhole radius [15]. In these simulations the pinhole radius was set to 3.2 μm.

The noise-free intensity value of the fluorophore in the detector plane was modeled as a Gaussian as in (4) with the parameter m determined by the fluorescence rate and the integration time (the time spent collecting photons at a single location). The total number of photons collected by the detector from the fluorescent probe was determined by integrating the exponential over the area of the pinhole and multiplying the result by the quantum efficiency of the detector. Background noise was introduced by adding a sample from a Poisson process with parameter $N_B = 10$ photons/ms. Finally, shot noise was included by adding a sample from a Poisson distribution whose parameter was given by the total number of photons collected by the detector. For a small circular pinhole, the SNR for the model taken here can be shown to be given approximately by [15]:

$$\text{SNR} = \sqrt{Q_E n_p}\frac{\pi r_d \text{N.A.}}{\lambda \text{M}\sqrt{1 + N_B/N}}$$

where N is the fluorescence rate of the molecule, λ is the wavelength of the emitted fluorescence, M is the magnification of the objective, Q_E is the quantum efficiency of the detector, and n_p is the total number of photons emitted by the molecule during the integration time. For all simulations, Q_E was set to 0.55 and an integration time of 15 ms was chosen, leading to a signal-to-noise ratio of 11.

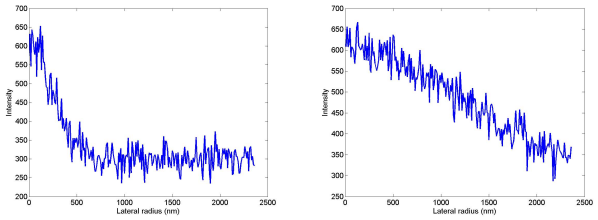

Fig. 1. Simulated intensity measurements with an SNR of 16.2. (left) Measurements along a radial line in the focal plane. (right) Measurements along a line in the axial direction with $(x, y) = (0, 0)$. The fluorophore is located at the origin.

The location of the fluorophore in each trial was chosen randomly from a uniform distribution on $x_0, y_0, z_0 \in$ [0 nm, 114 nm]. Intensity measurements were made from different positions in space. Measurements locations were chosen to be approximately evenly distributed over a sphere. Because the actual position of the fluorophore was unknown, the radial position of each measurement was selected randomly from the range $[0, r_d]$ where r_d is the radius of the pinhole, back-projected into the sample plane. This sampling pattern ensures that the intensity was measured at a variety of different ranges to the fluorescent probe.

In each trial the number of measurements was fixed and 100 iterations were run. For each run, the position of the fluorescent probe was determined from the data using the fluoroBancroft algorithm (12) as well as by using a nonlinear least-squares fit of the data to a Gaussian given by

$$I(x, y) = Ae^{-\frac{(x-x_0)^2+(y-y_0)^2}{2\sigma^2} - \frac{(z-z_0)^2}{2\sigma_z^2}}$$

in which x_0, y_0, z_0, A, σ and σ_z were allowed to vary. The simulations were performed in Matlab and the Gaussian fit performed using the built-in routine `lsqnonlin`.

IV. Results and Discussion

The execution time in Matlab for the fluoroBancroft algorithm was less than a millisecond even when 36 measurements were used and less than 300 μs when ten measurements were used. Because all calculations were done in Matlab, the execution times should be considered an upper bound. Fig. 2 shows the ratio of the Gaussian fit execution time to that of fluoroBancroft. In all cases the analytical algorithm is more than two orders of magnitude faster.

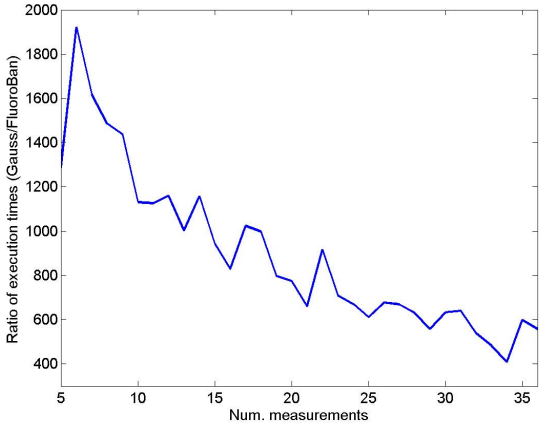

Fig. 2. Comparison of the execution times of the fluoroBancroft and Gaussian fitting algorithms. FluoroBancroft is at least two orders of magnitude faster than the fitting approach.

Fig. 3 shows the standard deviation in the error of the estimates, $\|\hat{r} - r_0\|$ where $\hat{r}$ is either the fluoroBancroft or Gaussian fit estimate. As the figure shows, the standard deviation of the Gaussian fit approach is greater than 500 nm in all cases. This is significantly higher than even the Rayleigh resolution criterion (approximately 400 nm for the given simulation parameters), indicating that the Gaussian fitting algorithm is unable to locate the fluorophore. However, the accuracy did improve as the number of measurements was increased and it is expected that with enough measurements, the algorithm would exceed the Rayleigh criterion. The fluoroBancroft algorithm successfully localized the fluorescent probe using only six measurements and had a standard deviation of less than 50 nm after only 9 measurements.

It is important to note that the choice of measurement locations has a large impact on the performance and statistical properties of the algorithm. Although this effect was not explicitly considered, this dependence is indicated in Fig. 4 in which the mean errors in the x, y, and z directions are shown. For an unbiased estimator, this mean should be zero. The figure shows that in these simulations, fluoroBancroft had a negative bias in all directions. There is therefore a need for further theoretical and experimental study to understand

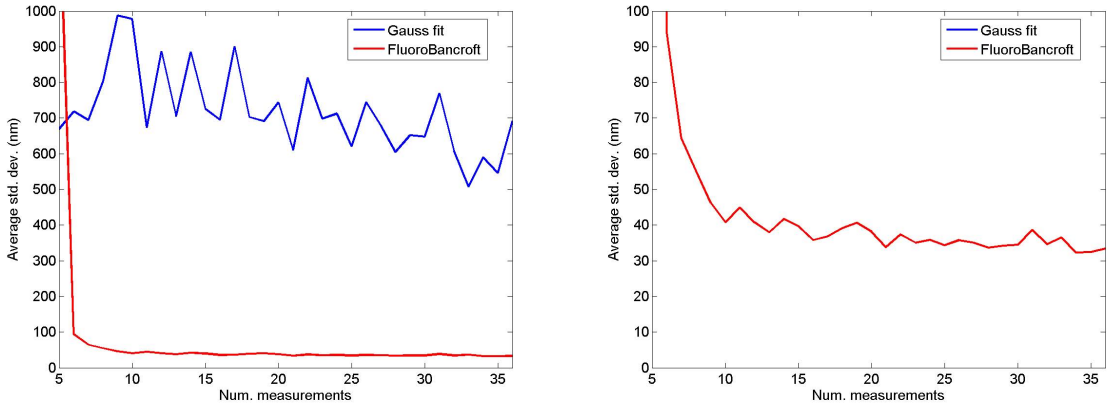

Fig. 3. Standard deviation of the error in the estimate of the position of the fluorescent probe as a function of the number of measurements. The bottom image is zoomed in on the vertical axis to indicate the performance of the fluoroBancroft algorithm. The simulations indicate that even with 36 measurements, the Gaussian algorithm has a standard deviation larger than the Rayleigh criterion, indicating the algorithm is not yielding any information. FluoroBancroft drops below the Rayleigh criterion using only six measurements and below 50 nm using only nine measurements.

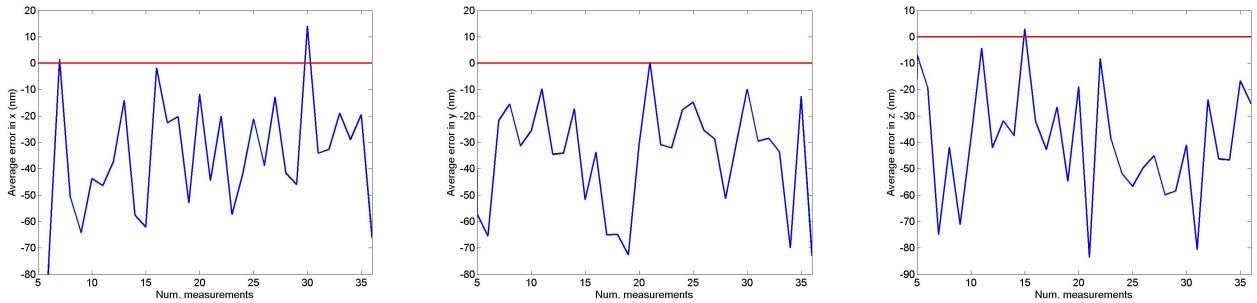

Fig. 4. Mean of the errors in the x (left), y (center), and z (right) axes. Because the measurement locations in the simulations changed as the number of measurements was varied, these results indicate that the choice of where to collect data has a strong influence on the accuracy of the results and that a bias can be introduced into the estimate depending on the choice of measurement locations.

the effect of the measurement locations and to design optimal sampling patterns.

REFERENCES

[1] M. K. Cheezum, W. F. Walker, and W. H. Guilford, "Quantitative comparison of algorithms for tracking single fluorescent particles," *Biophys. J.*, vol. 81, pp. 2378–2388, 2001.

[2] H. P. Babcock, C. Chen, and X. Zhuang, "Using single-particle tracking to study nuclear trafficking of viral genes," *Biophys. J.*, vol. 87, pp. 2749–2758, 2004.

[3] C. Kural, H. Kim, S. Syed, G. Goshima, V. I. Gelfand, and P. R. Selvin, "Kinesin and dynein move peroxisome in vivo: a tug-of-war or coordinated movement?" *Science*, vol. 308, no. 5727, pp. 1469–1472, June 2005.

[4] D. Thomann, D. R. Rines, P. K. Sorger, and G. Danuser, "Automatic fluorescent tag detection in 3D with super-resolution: application to the analysis of chromosome movement," *J. Microsc.*, vol. 208, no. 1, pp. 49–64, October 2002.

[5] V. Levi, Q. Ruan, and E. Gratton, "3-D particle tracking in a two-photon microscope application to the study of molecular dynamics in cells," *Biophys. J.*, vol. 88, pp. 2919–2928, 2005.

[6] A. J. Berglund and H. Mabuchi, "Feedback controller design for tracking a single fluorescent molecule," *Appl. Phys. B*, vol. 78, pp. 653–659, 2004.

[7] S. B. Andersson, "Tracking a single fluorescent molecule with a confocal microscope," *Appl. Phys. B*, vol. 80, no. 7, pp. 809–816, 2005.

[8] ——, "Precise localization fo fluorescent probes without numerical fitting," in *Proc. IEEE Int. Symp. Biomed. Imaging (ISBI)*, 2007, pp. 252–255.

[9] ——, "Position estimation of fluorescent probes in a confocal microscope," in *Proc. IEEE Conference on Decision and Control*, submitted, 2007.

[10] S. Bancroft, "An algebraic solution of the GPS pseudorange equations," *IEEE Trans. Aerosp. Electron. Syst.*, vol. AES-21, pp. 56–59, November 1985.

[11] E. S. W. R. J. Ober, S. Ram, "Localization accuracy in single molecule microscopy," *Biophys. J.*, vol. 86, pp. 1185–1200, 2004.

[12] R. E. Thompson, D. R. Larson, and W. W. Webb, "Precise nanometer localization analysis for individual fluorescent probes," *Biophys. J.*, vol. 82, pp. 2775–2783, 2002.

[13] C. Kural, H. Balci, and P. R. Selvin, "Molecular motors one at a time: FIONA to the rescue," *J. Phys. Condens. Matter*, vol. 17, pp. S3979–S3995, 2005.

[14] J. E. N. Jonkman and E. H. K. Stelzer, "Resolution and contrast in confocal and two-photon microscopy," in *Confocal and two-photon microscopy: Foundations, applications, and advances*, A. Diaspro, Ed. Wiley-Liss, 2002, ch. 5, pp. 101–126.

[15] C. J. R. Sheppard, X. Gan, M. Gu, and M. Roy, *Handbook of Biological Confocal Microscopy*, 3rd ed. Springer, 2006, ch. 22. Signal-to-noise ratio in confocal microscopes, pp. 442–452.